



## Controlled Shift in Emission Wavelength from Patterned Porous Silicon Using Focused Ion Beam Irradiation

D. Mangaiyarkarasi,<sup>a</sup> E. J. Teo,<sup>a</sup> M. B. H. Breese,<sup>a,z</sup> A. A. Bettiol,<sup>a</sup> and D. J. Blackwood<sup>b,\*</sup>

<sup>a</sup>Centre for Ion Beam Applications, Department of Physics, and <sup>b</sup>Department of Materials Science, National University of Singapore, Singapore 117542

Photoluminescence images containing several distinct color emissions, from green to red, have been obtained using high-energy focused ion beam irradiation, in conjunction with metal-aided anodization of 4  $\Omega$  cm p-type silicon. The ion irradiation increases the local resistivity in a controlled manner resulting in smaller hole currents flow through the irradiated areas. This causes a controlled redshift of up to 200 nm in the photoluminescence emission, which in terms of the quantum confinement model would correlate to larger nanocrystallites forming in the irradiated region.

© 2005 The Electrochemical Society. [DOI: 10.1149/1.2032347] All rights reserved.

Manuscript submitted April 15, 2005; revised manuscript received May 31, 2005. Available electronically August 25, 2005.

The observation of visible light emission due to quantum confinement from electrochemically etched porous silicon (PSi)<sup>1</sup> and silicon nanocrystals provides a possibility for the development of silicon-based light emitting devices<sup>2</sup> and silicon lasers<sup>3</sup> for optoelectronic applications. Extensive studies have been carried out to understand the photoluminescence (PL) mechanisms<sup>4-6</sup> as well as to control and pattern light-emitting regions of nanocrystalline silicon with acceptable lithographic resolution for monolithic Si-based integrated optoelectronic<sup>7,8</sup> and photonic<sup>9</sup> devices.

There have been many attempts to pattern porous silicon using photolithography,<sup>10,11</sup> electron beam lithography,<sup>12</sup> soft lithography,<sup>13</sup> doping-induced selectivity,<sup>14</sup> focused heavy ion beams,<sup>15</sup> and amorphization-controlled selectivity.<sup>16</sup> We have recently reported direct-write patterning of PSi to produce micrometer-sized areas with variable intensity red PL emission using focused, high-energy proton irradiation of low resistivity (0.02  $\Omega$  cm) p-type silicon.<sup>17</sup> The focused ion beam creates lattice defects at the irradiated regions, which increases the local resistivity. Low resistivity silicon tends to produce PSi, which emits low-intensity PL due to excessive charge carrier concentration.<sup>18,19</sup> At ion-irradiated regions, the increased resistivity results in PSi, which emits more intense PL due to the lower carrier concentration than in the substrate. In contrast, higher resistivity silicon (1–10  $\Omega$  cm) usually exhibits efficient PL intensity, whereas ion irradiated regions produce fainter, redshifted PL since these areas are very resistive. In terms of the quantum confinement model, a redshift in the PL corresponds to an increase in the size of the nanocrystallites responsible for its existence.<sup>18</sup> The influence of wafer resistivity on the crystallite size of porous silicon produced by anodization has been previously studied.<sup>19</sup>

Many efforts have been made on high resistivity Si to alter the peak wavelength emission from PSi, such as oxidation<sup>20</sup> or photochemical etching<sup>21,22</sup> or doping with rare-earth compounds.<sup>23</sup> Recently, Kim et al.<sup>24,25</sup> reported PL over the full visible range from 1 to 10  $\Omega$  cm p-type PSi using electrochemical etching aided by an oxidative metal (i.e., one with a reduction potential lower than that of hydrogen) such as Zn or Fe. A monotonic decrease in PL wavelength from 620 to 430 nm as the etching current density was increased from 20 to 100 mA/cm<sup>2</sup> was reported. One mechanism by which this may occur is the following: when powdered Zn is added to the HF electrolyte it corrodes, liberating hydrogen and causing an increase in pH. This will have the overall effect of reducing the HF<sub>2</sub><sup>-</sup> concentration,<sup>19</sup> favoring the formation of surface oxides/hydroxides which can emit blue/green PL. Another possible mechanism is nanocrystalline silicates formed within the porous layer.<sup>26</sup>

However, producing a wide range of wavelength emission on the adjacent areas of a single Si substrate in a controlled manner is a

challenging task. In this work, we employed a novel approach to controllably alter the PL peak wavelength emission from adjacent, micrometer sized areas of PSi using high-energy, focused ion beam irradiation in conjunction with metal-aided anodization. Ion irradiation increases the local resistivity in a controlled manner, resulting in smaller hole current flowing through the irradiated regions during metal aided anodization with high current density. The peak PL wavelength at the unirradiated regions has a short wavelength, typically green, whereas PL at the irradiated regions is controllably redshifted by increasing the ion dose. This causes controlled redshift of up to 200 nm in the PL emission, which in terms of the quantum confinement model would correlate with larger nanocrystallites forming in the irradiated region. This results in PL images containing several distinct color emissions, from green to red.

### Experimental

p-type Si (100) wafers, with resistivity of 4  $\Omega$  cm, were used in this present study. High-energy ion irradiation was carried out to pattern Si samples using the National University of Singapore nuclear microprobe,<sup>27,28</sup> which can focus MeV ion beams to spot sizes < 100 nm. An electrical contact was made to the back surface using Ga–In eutectic and copper wire. Epoxy resin was used to protect the contact from the HF. The anodization was done at a constant current density of 100 mA/cm<sup>2</sup> in a solution of HF:H<sub>2</sub>O:C<sub>2</sub>H<sub>5</sub>OH (1:1:2 by volume), with an additional Zn metal concentration of 10<sup>-3</sup> mol/L dissolved in the electrolyte.

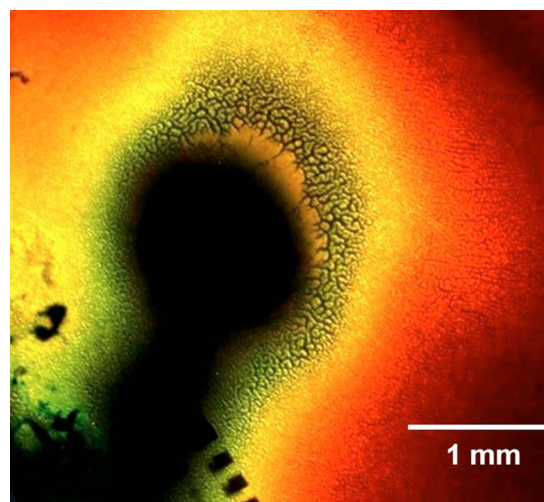
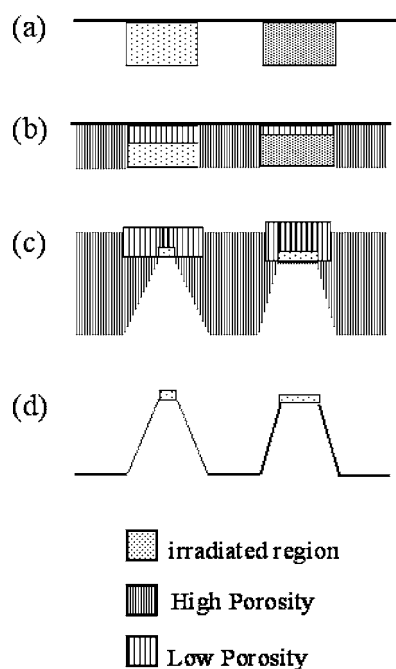


Figure 1. Large-area PL image of a 4  $\Omega$  cm p-type wafer after metal-aided anodization.

\* Electrochemical Society Active Member.

<sup>z</sup> E-mail: phymbhb@nus.edu.sg



**Figure 2.** Schematic of the metal-aided anodization process. (a) Ion irradiation with a low/high dose on the left/right side. (b) After a short anodization period. (c) After a long anodization period. (d) After immersion in KOH.

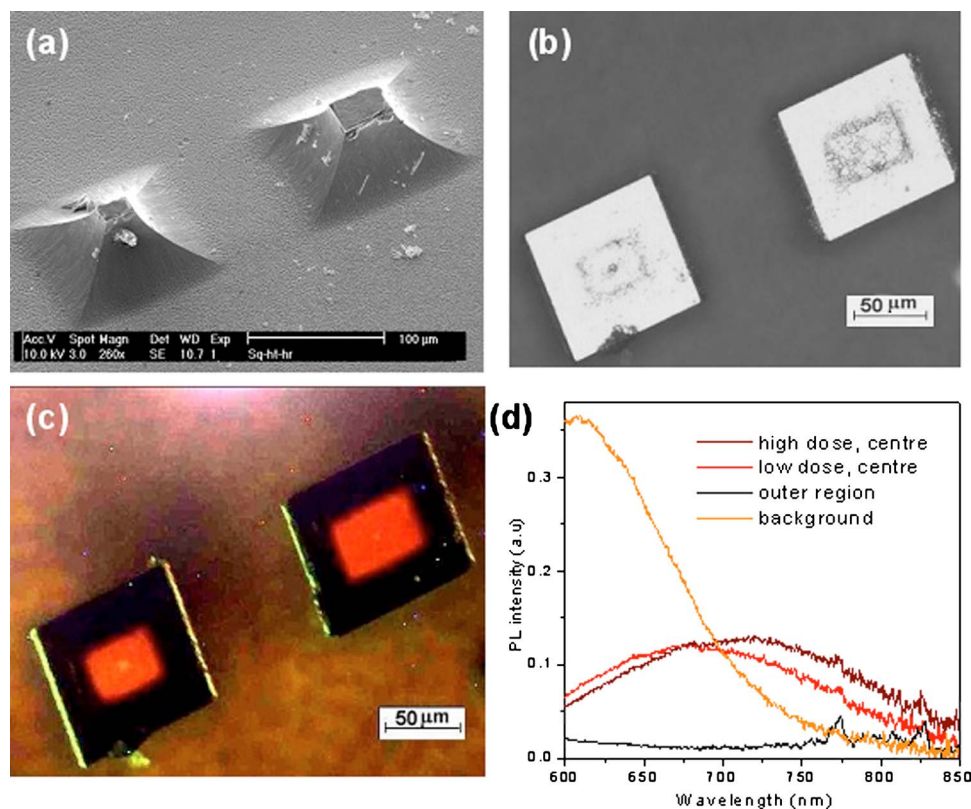
A high-resolution optical microscope (Nikon Eclipse ME600) was used to image the PL at the micrometer-sized irradiated regions with UV excitation. A long pass filter with a pass band above 570 nm was used to cut out the excitation wavelength, so only PL was collected by a CCD camera. Also micro PL spectra measurements were performed using a Leica DMLM microscope attached

with a CCD Ocean Optics spectrometer via an optic fiber. The 532 nm light from a diode pumped solid-state laser of 1-2 mW power was focused onto the sample through a  $\times 50$  objective lens. PL emission was detected by the spectrometer after passing through a red dichroic filter and 550-nm-long pass filter to remove the excitation light and the spectra corrected for system response. A scanning electron microscope (Phillips XL30 FEG) was used to examine the morphology of irradiated structures after removal of PSi in KOH (potassium hydroxide) solution.

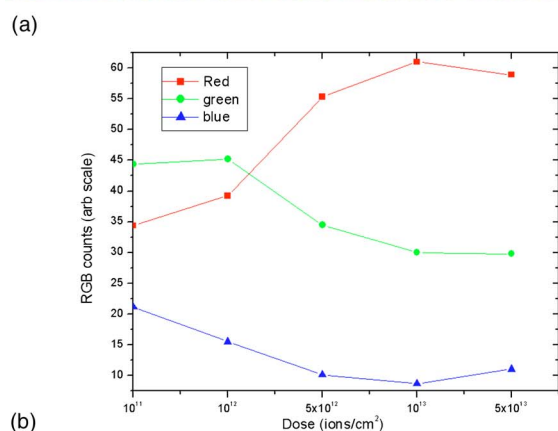
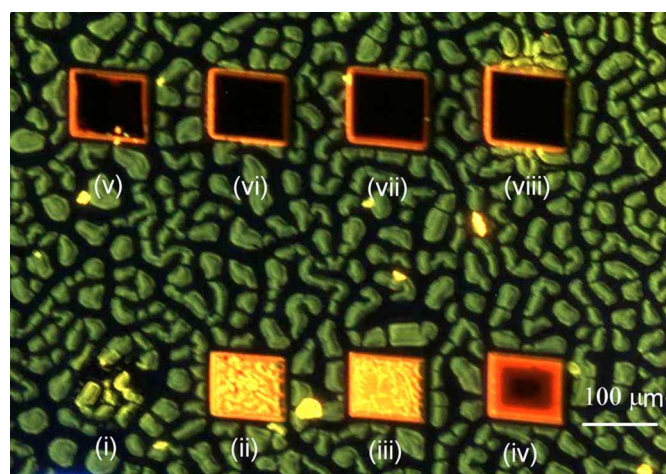
## Results and Discussion

Figure 1 demonstrates the wide range of PL wavelengths, which can be produced with a small-area contact made to the rear surface of an unirradiated silicon wafer. This results in a nonuniform current density across the surface during anodization, producing a range of different color PL emission. Exposure to air rapidly redshifted the PL from green to yellow, so after anodization the samples were rinsed in ethanol and immediately transferred to a vacuum chamber to minimize atmospheric oxidation.

Squares of  $100 \times 100 \mu\text{m}^2$  area were irradiated with different doses of 1 MeV helium ions and protons, as shown in Fig. 2a. The ions lose energy as they penetrate the silicon and come to rest at a well-defined range, equal to  $\sim 4 \mu\text{m}$  for 1 MeV helium ions and  $\sim 15 \mu\text{m}$  for 1 MeV protons. Unlike in Fig. 1, a single wavelength emission across the unirradiated regions may be easily achieved with a uniform electrical contact to the backside of the sample. After anodization for a short period (Fig. 2b), regions away from the irradiated area become porous. The irradiated regions etch at a lower rate, depending on the dose, producing material with a lower porosity. The outer portions of the irradiated areas still transport a small hole current, so these areas have porosity higher than the central portions. After anodization for a longer period (Fig. 2c), the silicon wafer is etched beyond the end of the ion range. Central portions of the irradiated areas can transport a larger hole current than the undercut outer



**Figure 3.** Two irradiated squares, irradiated with doses of  $2$  and  $4 \times 10^{14}/\text{cm}^2$  1 MeV He ions, to the left/right side. (a) SEM after removal of PSi by immersion in KOH. (b) Reflected light image and (c) PL image, focused on the higher irradiated surfaces. (d) PL spectra recorded from the unirradiated, background area, two from the inner centers and one from the outer region of the irradiated squares.



**Figure 4.** (a) PL image of eight squares, irradiated with 1 MeV proton doses of (i)  $10^{12}$ , (ii)  $5 \times 10^{12}$ , (iii)  $10^{13}$ , (iv)  $5 \times 10^{13}$ , (v)  $10^{14}$ , (vi)  $5 \times 10^{14}$ , (vii)  $10^{15}$ , and (viii)  $5 \times 10^{15}$  ions/cm<sup>2</sup>. PL was collected by a CCD camera with a long pass filter with a pass band above 470 nm to cut out the peak excitation wavelength of 370 nm. (b) Change in red, green, blue components of the PL measured from each irradiated square in (a), as a function of dose.

portions, hence they have a higher porosity. If the anodized sample is immersed in KOH, all PSi is removed, resulting in a patterned wafer surface as in Fig. 2d.

Two squares were irradiated with doses of  $2$  and  $4 \times 10^{14}$ /cm<sup>2</sup> 1 MeV He ions. Figure 3a shows an SEM image of the regions remaining after metal-aided anodization for 8 min at a current density of 100 mA/cm<sup>2</sup>, and subsequent immersion in KOH, i.e., at a stage corresponding to Fig. 2d. The irradiated areas have been undercut on all sides due to isotropic etching and are eventually etched away, but the central portions still remain attached to the substrate, as discussed above. PL images and spectra of this anodized structure were recorded before immersion in KOH, i.e., at a stage corresponding to Fig. 2c. Such anodization conditions produce intense green PL emission at the unirradiated areas if stored in vacuum. However, the geometry of the vacuum chamber was not compatible with high-resolution optical microscopy or micro-PL measurements, so the samples were subsequently analyzed in air. This introduced a redshift of the background PL from the unirradiated areas, with green PL turning yellow. Figure 3b and c shows a reflected light and a PL image of the two irradiated squares captured using an optical microscope. Yellow PL is observed in the unirradiated background, and uniform, intense red PL is observed from the central portions of the irradiated squares. These central portions are also visible in the reflected image in Fig. 3b. The square irradiated with a higher dose is less undercut, hence PL emission is observed over a larger area.

In Fig. 3d, the micro-PL spectrum from the unirradiated background has a peak wavelength at  $\sim 610$  nm. The PL spectra recorded from the centers of the squares have peak wavelengths from 680 to 720 nm, i.e., redshifted by 70–110 nm with respect to the unirradiated background, owing to the lower hole current flowing through these regions. The peak emission from the higher dose irradiation is more redshifted, again consistent with a lower hole current. We note that the redshift at the irradiated regions would be  $\sim 200$  nm if measured in vacuum, with the unirradiated background region remaining green. No PL is observed from the outer, undercut areas of the irradiated squares in Fig. 3. In these outer areas, a small hole current flows, producing PSi with a porosity too low to exhibit visible PL. These outer regions are removed after immersions in KOH and so are absent in Fig. 3a.

Figure 4a shows a PL image of a PSi wafer where eight squares were irradiated with 1 MeV protons over a wide range of doses. Figure 4b shows the corresponding change in the red, green, and blue components of the PL measured from the irradiated squares. The wafer underwent metal anodization for 6 min. The shorter anodization time and longer proton range results in the irradiated regions not becoming undercut, similar to Fig. 2b. Here it was possible to record a PL image in air before the background underwent a significant redshift, resulting in a graphic demonstration of controlled redshifting. The lowest four irradiation doses produce yellow, yellow/orange, orange/red, and red PL respectively. Above a certain dose, red PL is observed only at the irradiated edges, where the hole current is not reduced to zero. Formation of porous silicon during metal-aided anodization typically leads to a more amorphous structure and higher strain in the film due to the oxide-related defects.<sup>24,25</sup> This can be seen in Fig. 4a, where the unirradiated background is granular.

In conclusion, focused ion beam irradiation in conjunction with metal-aided anodization can achieve short-wavelength PL emission at unirradiated regions and controlled, redshifted PL at ion-irradiated regions, with the shift depending on the ion dose. As mentioned in the introduction to this paper, in terms of the quantum confinement model, a redshift correlates to larger nanocrystallites. It is then postulated that the redshift observed in the irradiated region is also due to the formation of large nanocrystallites forming in the irradiated region. However, no direct evidence of this was obtained.

The use of focused ion beam irradiation may provide great flexibility in shaping future devices. We are currently adapting this approach to other methods of producing short-wavelength PL, such as photochemical etching. For optoelectronic applications such as full-color display and optical interconnection, this process could provide tuneable controlled light emission from adjacent, micrometer sized areas of porous silicon with utilizable efficiency across the whole visible light range.

National University of Singapore assisted in meeting the publication costs of this article.

## References

1. L. T. Canham, *Appl. Phys. Lett.*, **57**, 1046 (1990).
2. S. Chan and P. M. Fauchet, *Appl. Phys. Lett.*, **75**, 274 (1999).
3. L. Pavesi, L. Dal Negro, C. Mazzoleni, G. Franzo, and F. Priolo, *Nature (London)*, **408**, 440 (2000).
4. A. G. Cullis, L. T. Canham, and P. D. J. Calcott, *J. Appl. Phys.*, **82**, 909 (1997).
5. S. Ossicini, L. Pavesi, and F. Priolo, *Light Emitting Silicon for Microphotonics*, SMTP, 194, pp. 75–122, Springer-Verlag, Berlin (2003).
6. D. W. Cooke, R. E. Muenchausen, B. L. Bennett, L. G. Jacobsohn, and M. Nastasi, *J. Appl. Phys.*, **96**, 197 (2004).
7. K. D. Hirschman, L. Tsybeskov, S. P. Duttagupta, and P. M. Fauchet, *Nature (London)*, **384**, 338 (1996).
8. G. Barillaro, A. Diligenti, F. Pieri, F. Fuso, and M. Allegrini, *Appl. Phys. Lett.*, **78**, 4154 (2001).
9. A. Briner, R. B. Wehrspohn, U. M. Gösele, and K. Busch, *Adv. Mater. (Weinheim, Ger.)*, **13**, 377 (2001).
10. V. V. Doan and M. J. Sailor, *Science*, **256**, 1791 (1992).
11. A. Givant, J. Shappir, and A. Sa'ar, *Appl. Phys. Lett.*, **73**, 3150 (1998).
12. S. Borini, A. M. Rossi, L. Boarino, and G. Amato, *J. Electrochem. Soc.*, **150**, G311 (2003).
13. D. J. Sirbully, G. M. Lowman, B. Scott, G. D. Stucky, and S. K. Buratto, *Adv. Mater. (Weinheim, Ger.)*, **15**, 149 (2003).

14. A. J. Steckl, J. Xu, H. C. Mogul, and S. Mogren, *Appl. Phys. Lett.*, **62**, 1982 (1993).
15. P. Schmuki, L. E. Erickson, and D. J. Lockwood, *Phys. Rev. Lett.*, **80**, 4060 (1998).
16. S. P. Duttgupta, C. Peng, and P. M. Fauchet, S. K. Kurinec, and T. N. Blanton, *J. Vac. Sci. Technol. B*, **13**, 1230 (1995).
17. E. J. Teo, D. Mangaiyakarasi, M. B. H. Breese, A. A. Bettiol, and D. J. Blackwood, *Appl. Phys. Lett.*, **85**, 4370 (2004).
18. V. Lehmann, *The Electrochemistry of Silicon: Instrumentation, Science, Materials and Applications*, Wiley-VCH, New York (2002).
19. Z. Gaburro, H. You, and D. Babić, *J. Appl. Phys.*, **84**, 6345 (1998).
20. A. J. Kontkiewicz, A. M. Kontkiewicz, J. Siejka, S. Sen, G. Nowak, A. M. Hoff, P. Sakthivel, K. Ahmed, P. Mukherjee, S. Witanachchi, and J. Lagowski, *Appl. Phys. Lett.*, **65**, 1436 (1994).
21. H. Mizuno, H. Koyama, and N. Koshida, *Appl. Phys. Lett.*, **69**, 3779 (1996).
22. M. V. Wolkin, J. Jorne, P. M. Fauchet, G. Allan, and C. Delerue, *Phys. Rev. Lett.*, **82**, 197 (1999).
23. L. Luo, X. X. Zhang, K. F. Li, K. W. Cheah, J. X. Shi, W. K. Wong, and M. L. Gong, *Adv. Mater. (Weinheim, Ger.)*, **16**, 1664 (2004).
24. K. Y. Suh, Y. S. Kim, S. Y. Park, and H. H. Lee, *J. Electrochem. Soc.*, **148**, C439 (2001).
25. Y. S. Kim, K. Y. Suh, H. Yoon, and H. H. Lee, *J. Electrochem. Soc.*, **149**, C50 (2002).
26. N. Taghavinia, G. Lerondel, H. Makino, A. Yamamoto, T. Yao, Y. Kawazoe, and T. Goto, *Nanotechnology*, **12**, 547 (2001).
27. J. A. van Kan, A. A. Bettiol, and F. Watt, *Appl. Phys. Lett.*, **83**, 1629 (2003).
28. E. J. Teo, M. B. H. Breese, E. P. Tavernier, A. A. Bettiol, F. Watt, M. H. Liu, and D. J. Blackwood, *Appl. Phys. Lett.*, **84**, 3202 (2004).